

This discussion paper is/has been under review for the journal Atmospheric Measurement Techniques (AMT). Please refer to the corresponding final paper in AMT if available.

**OZORAM –  
stratospheric  
O<sub>3</sub> above the Arctic**

M. Palm et al.

# The ground-based MW radiometer OZORAM on Spitsbergen – description and validation of stratospheric and mesospheric O<sub>3</sub>-measurements

M. Palm, C. G. Hoffmann, S. H. W. Golchert, and J. Notholt

IUP, Universität Bremen, Bremen, Germany

Received: 5 March 2010 – Accepted: 12 April 2010 – Published: 22 April 2010

Correspondence to: M. Palm (mathias@iup.physik.uni-bremen.de)

Published by Copernicus Publications on behalf of the European Geosciences Union.

Title Page

Abstract

Introduction

Conclusions

References

Tables

Figures

⏪

⏩

◀

▶

Back

Close

Full Screen / Esc

Printer-friendly Version

Interactive Discussion



## Abstract

This manuscript introduces the OZORAM ground based millimeter wave radiometer. The instrument is deployed to the high Arctic (79° N, 12° E) for measurements of O<sub>3</sub> in the upper stratosphere and lower mesosphere.

5 The discussion covers measurements taken since late 2006. To investigate instrumental biases, the results from September 2008 till spring 2009 are compared to O<sub>3</sub> profiles derived from measurements of two instruments onboard polar orbiting satellites, MLS onboard EOS-AURA and SABER onboard TIMED. The agreement is within 20% in the stratosphere and 40% in the mesosphere. The deviations show strong  
10 systematic and oscillating features, for which the error discussion of the ground based instrument/measurement gives possible explanations.

Nonetheless, expected features like the diurnal cycle and O<sub>3</sub> enhancements due to stratospheric warmings are readily observed, which could not originally be taken for granted given the large deviation from the satellite data.

15 The nature of the oscillatory deviation is further studied. This study points to a systematic error in the radiative transfer modeling caused by imperfect spectroscopic data.

## 1 Introduction

20 O<sub>3</sub> is an atmospheric component of major interest. The stratosphere, synonymous with the O<sub>3</sub> layer filters most of the UV radiation and thus enables life on Earth outside water. While the O<sub>3</sub> layer, and its depletion due to anthropogenically released chemicals, was a major research topic throughout the 1990s, the focus of O<sub>3</sub> research has recently shifted upwards towards the upper stratosphere and the mesosphere.

25 The mesosphere/lower thermosphere (MLT-region) forms the interface between atmosphere and outer space. Radiation and particles from the sun and outer space enter the MLT-region and release their energy there or even penetrate into the upper

AMTD

3, 1933–1970, 2010

## OZORAM – stratomesospheric O<sub>3</sub> above the Arctic

M. Palm et al.

Title Page

Abstract

Introduction

Conclusions

References

Tables

Figures

⏪

⏩

◀

▶

Back

Close

Full Screen / Esc

Printer-friendly Version

Interactive Discussion



stratosphere. They trigger a whole class of chemical reactions, the ion chemistry, which leads to the formation of hydrogen and nitrogen radicals. While hydrogen radicals are most effective in the lower mesosphere (Lary, 1997) and decay on a timescale of hours to days, nitrogen radicals travel deep into the stratosphere by large scale descent of mesospheric and thermospheric air during polar winter (Randall et al., 2005). Nitrogen radicals become effective in O<sub>3</sub> destruction in the upper stratosphere (Lary, 1997). Hence, solar activity can exert strong influence on the stratospheric chemistry and on the O<sub>3</sub>-layer.

O<sub>3</sub> is involved in much of the atmospheric chemistry. It is sensitive to changes in irradiation. The information about its distribution in the atmosphere is easily accessible due to its numerous molecular transitions causing strong absorption throughout the IR-spectrum. Measurements in the far infrared, corresponding to wavelengths in the mm-range, are particularly suited to mesospheric studies using passive ground-based measurements because profile information can be accessed well into the lower mesosphere.

Passive millimeter wave measurements of atmospheric trace gases offer a range of unique features. They are independent of solar or lunar irradiation and largely insensitive to weather conditions. The measurements have a good time resolution of less than 1 h and capture a narrow and well defined trace through the atmosphere.

This publication describes mostly instrumental aspects of the **Ozone Radiometer for Atmospheric Measurements (OZORAM)**, a ground based microwave radiometer located on the Spitsbergen archipelago. The instrument has been modified to enable measurements of mesospheric O<sub>3</sub>. Section 2 describes the instrument and the retrieval methods for drawing information from the measurements. A retrieval assessment and an error characterization of the measurements conclude this section.

Section 3 presents the data set obtained since autumn 2006. This includes a characterization of the measurement geometry and a discussion of some outstanding features.

The data available from autumn 2008 until spring 2009 are compared to two space

## OZORAM – stratomesospheric O<sub>3</sub> above the Arctic

M. Palm et al.

Title Page

Abstract

Introduction

Conclusions

References

Tables

Figures

◀

▶

◀

▶

Back

Close

Full Screen / Esc

Printer-friendly Version

Interactive Discussion



borne instruments that measure the polar winter atmosphere, i.e. MLS onboard the AURA-EOS satellite (Schoeberl et al., 2006) and SABER onboard the TIMED satellite (Russel et al., 1994) in Sect. 4. This study indicates some instrumental bias in OZORAM. Section 5 investigates the nature of the so-called oscillations in the retrieved O<sub>3</sub> profiles.

## 2 The OZORAM instrument

### 2.1 General

The OZORAM instrument is located at the AWIPEV research base in Ny Ålesund (79.9° N, 11.9° E) on the Spitsbergen archipelago. It is commonly operated by the Alfred Wegener Institute (AWI) and the Universität Bremen. It has been committed to operation in 1994 (Sinnhuber et al., 1998) and has been modified for measurements of mesospheric emissions in 2006–2008 (for a history of the instrument see Table 1).

### 2.2 The ground based millimeter wave radiometer OZORAM

This publication does not account for the status of the instrument before 2006. During summers 2006, 2007 and 2008, several modifications and optimizations were carried out in order to extend observations into the mesosphere. Between 2006 and 2008 the data have different performance specifications, which are reported separately in Table 1. Since autumn 2008 the OZORAM is fully operational in the mesosphere mode.

The OZORAM is a heterodyne single side-band receiver tuned to the 142.176 GHz emission line ( $10_{1,9} \rightarrow 10_{0,10}$ ) of O<sub>3</sub>. The bandwidth is 800 MHz and the frequency resolution is approx. 60 kHz. Its main building blocks are (compare also Fig. 1):

*Frontend.* It consists of a quasi optical system and Schottky mixer followed by a low noise HEMT amplifier. The quasioptical system selects the radiation source from hot black body, cold black body or the atmosphere, respectively. A Martin-Puplett-interferometer is used to

## OZORAM – stratospheric O<sub>3</sub> above the Arctic

M. Palm et al.

Title Page

Abstract

Introduction

Conclusions

References

Tables

Figures

◀

▶

◀

▶

Back

Close

Full Screen / Esc

Printer-friendly Version

Interactive Discussion



suppress the mirror side band at 126 GHz. The signal is down-converted to 8 GHz intermediate frequency.

*IF chain.* It is responsible for filtering, amplification, and further down conversion of the 8 GHz signal to be suitable as input to the spectrometer (DC – 1 GHz).

- 5 *Spectrometer.* The Fast-Fourier-transform (FFT) spectrometer Agilent AC240 (Benz et al., 2005) comprises fast AD converters and an FPGA (field programmable array)-implemented Fourier transformer. It delivers a bandwidth of 1 GHz and a resolution of approx. 60 kHz. The Fourier transformation is calculated in real time.

10 The OZORAM is operated in total power mode, alternately taking spectra from a hot black body,  $y_H$  ( $T_H = 293$  K), the atmosphere,  $y_A$ , and a cold black body,  $y_C$  ( $T_C = 77$  K). The black body spectra,  $y_H$  and  $y_C$ , are recorded for calibration purposes. The calibrated spectrum,  $y$ , can be calculated using the Planck formula,  $B_T$ , for black body radiation at temperature  $T$ :

$$y = \frac{B_{T_H} - B_{T_C}}{y_H - y_C} (y_A - y_C) + B_{T_C} \quad (1)$$

15 The receiver can be characterized via the receiver-noise-temperature,  $T_{REC}$ , which quantifies the noise contribution of the instrument to the measurement (Janssen, 1993). The standard deviation of the noise on the measurement,  $\sigma_y$ , can be estimated via the radiometric formula:

$$\sigma_y = \frac{T_{SYS}}{\sqrt{\nu t}} \quad \text{where} \quad T_{SYS} = T_{SIG} + T_{REC} \quad (2)$$

20 with the bandwidth,  $\nu$ , the integration time,  $t$  and the signal  $T_{SIG}$ . See Fig. 2 for an example of a calibrated spectrum and Fig. 3 for the profile retrieved from it (refer to Sect. 2.4 for a description of the retrieval). The night time profile exhibits the typical enhancement expected in mesospheric  $O_3$  in the absence of solar illumination.

## OZORAM – stratospheric $O_3$ above the Arctic

M. Palm et al.

Title Page

Abstract

Introduction

Conclusions

References

Tables

Figures

◀

▶

◀

▶

Back

Close

Full Screen / Esc

Printer-friendly Version

Interactive Discussion



---

**OZORAM –  
stratospheric  
O<sub>3</sub> above the Arctic**M. Palm et al.

---

[Title Page](#)[Abstract](#)[Introduction](#)[Conclusions](#)[References](#)[Tables](#)[Figures](#)[◀](#)[▶](#)[◀](#)[▶](#)[Back](#)[Close](#)[Full Screen / Esc](#)[Printer-friendly Version](#)[Interactive Discussion](#)

During the winter 2006/07 an acousto-optical-spectrometer (AOS) covered the broad band portion of the spectrum, in parallel to a chirp-transform-spectrometer (CTS) spectrometer resolving the line center. This combination has been used because the resolution of the AOS was not sufficient to resolve the mesospheric information at the line center. Due to permanent failure of the AOS spectrometer, this combination was replaced later by the FFT spectrometer.

From 2006 through 2008, the spectra were recorded within time intervals of 20 min alternating with a frontend tuned to the 22.2 GHz emission line of a water vapor transition. Prior to 2008, only about one third of the available time was used for O<sub>3</sub> measurements, which significantly reduces the SNR. This explains the difference in the maximum upper altitude reported in Table 1, 3rd column. Since autumn 2008, the system is only used for O<sub>3</sub> measurements. On-disk spectra are integrated for 10 min. In order to achieve a sufficient SNR, the spectra are further integrated, so that one spectrum is available per hour.

### 2.3 Radiative transfer

Radiative transfer is encoded in the forward model ARTS<sup>1</sup> (Bühler et al., 2005) and is only cursorily described in order to make the error analysis understandable. For a detailed account of the radiative transfer theory the reader is referred to any textbook dealing with the matter (e.g. Janssen, 1993).

Formally spoken, the forward model denotes a function,  $\mathbf{y} = F(\mathbf{x}, \mathbf{b})$ , which yields a spectrum,  $\mathbf{y}$ , for a given atmospheric state,  $\mathbf{x}$ , and a set of auxiliary parameters,  $\mathbf{b}$ . The atmospheric state comprises one or several trace gas profiles, usually given on a pressure grid. The auxiliary parameters include an atmospheric temperature profile, spectroscopic data of the observed transitions, and parameters of the instrument.

The formulas for the radiative transfer are documented in the ARTS user guide (part of the ARTS package) version 1.0.216.

---

<sup>1</sup>Available for download at <http://www.sat.ltu.se/>

### 2.3.1 Absorption and emission in a fixed layer

The absorption at a point in the atmosphere, here represented by a given pressure  $p$ , and a given frequency  $\nu$ , corresponds to

$$\alpha(p, \nu) = x(p)S(T)L(\nu, p, T), \quad (3)$$

5 where  $x(p)$  denotes the amount of the observed trace gas at pressure  $p$ ,  $S(T)$  denotes the strength of the considered transition, depending on the temperature, and  $L(\nu, p, T)$ , the so called line shape factor which also depends on frequency,  $\nu$ , pressure,  $p$ , and temperature,  $T$ . The data necessary to calculate those contributions are tabulated in spectral databases, e.g. HITRAN, version 2004 (Rothman et al., 2005) or JPL, version 2009 (Pickett et al., 1998), both of which have been used in this work.

The line strength is calculated via

$$S(T) = S(T_0) \frac{Q(T_0)}{Q_T} \frac{\exp\left(-\frac{E_u}{kT}\right) - \exp\left(-\frac{E_l}{kT}\right)}{\exp\left(-\frac{E_u}{kT_0}\right) - \exp\left(-\frac{E_l}{kT_0}\right)} \quad (4)$$

using the Boltzmann factor  $k$ . The line strength  $S(T_0)$ , the partition function  $Q(T)$ , and the lower state energy  $E_l$  are tabulated. Using the frequency of the transition,  $\nu_0$ , the upper state energy,  $E_u$ , is given by  $E_u = h\nu_0 + E_l$ .

The line shape describes the alteration of the monochromatic radiation due to interactions of the molecule with its environment. Most notable are collisions with molecules of the same or other species (pressure induced) and movements due to kinetic energy, i.e. temperature. The line shape can be described using the Voigt function (Janssen, 1993). The pressure induced line shape is defined via a pressure broadening parameter,  $\gamma_{\text{AIR}}$ , which is tabulated for a single temperature,  $T_0$ , and can be extrapolated to an arbitrary temperature via

$$\gamma_{\text{AIR}}(T) = \gamma_{\text{AIR}}(T_0) \rho \left( \frac{T_0}{T} \right)^{n_{\text{AIR}}} \quad (5)$$

Title Page

Abstract

Introduction

Conclusions

References

Tables

Figures

◀

▶

◀

▶

Back

Close

Full Screen / Esc

Printer-friendly Version

Interactive Discussion



using the tabulated parameter  $n_{\text{AIR}}$ .

### 2.3.2 The modeling of the spectrum

Emission  $\epsilon$  and absorption  $\alpha$  are connected via Kirchhoff's law:

$$\frac{\epsilon}{\alpha} = B_T \quad (6)$$

- 5 with  $B_T$  the Planck function for the temperature  $T$ . The spectrum itself,  $y$ , is created by a sum of the emission and absorption along the line of sight from the sensor location,  $s_0$ , to the top of the atmosphere,  $s_\infty$ . It is calculated via:

$$y = F(\mathbf{x}, \mathbf{b}) = y_\infty \exp(-\tau(s_0, s_\infty)) + \int_{s_0}^{s_\infty} \underbrace{\alpha(s)B(T)}_{\text{Emission}} \overbrace{\exp(-\tau(s_0, s))}^{\text{Absorption}} ds. \quad (7)$$

- 10 The spectrum measured at  $s_\infty$ , here the Planck radiation of space, is denoted by  $y_\infty$ .  $\tau(s_1, s_2) = \int_{s_1}^{s_2} \alpha(s) ds$  is the absorption between  $s_1$  and  $s_2$  along the line of sight.  $\mathbf{x}$  is the profile of the species under consideration.

### 2.3.3 Summary of the radiative transfer

- 15 These elements of radiative transfer are stated because they are of importance in the discussion to follow:

1. For the 142 GHz  $\text{O}_3$  emission, the pressure determines the line-width up to an altitude of about 55 km. Above 65 km it is governed by temperature. In the range between it is determined by a mixture of both effects occurs which is commonly represented in the Voigt line shape (Janssen, 1993).

Title Page

Abstract

Introduction

Conclusions

References

Tables

Figures

◀

▶

◀

▶

Back

Close

Full Screen / Esc

Printer-friendly Version

Interactive Discussion



2. Roughly, the height of the emission line corresponds to the volume-mixing-ratio (VMR) of the trace gas (this is strictly true in the pressure broadening regime (Janssen, 1993, Sect. 2.4.2)). The area beneath the emission line corresponds to the number of molecules in a fixed volume.

3. The radiation created in a given altitude is attenuated by the absorption in lower altitudes.

## 2.4 The retrieval

### 2.4.1 Retrieval setup

The spectra are analyzed using the optimal estimation method (Rodgers, 2000). Optimal estimation is a statistically founded method in which the result,  $\hat{\mathbf{x}}$ , given the measurement,  $\mathbf{y}$ , is the largest value of the conditional probability density

$$\rho(\hat{\mathbf{x}}|\mathbf{y}) \sim \exp\left(-(\mathbf{F}(\hat{\mathbf{x}}) - \mathbf{y})\mathbf{S}_e^{-1}(\mathbf{F}(\hat{\mathbf{x}}) - \mathbf{y})^T\right) \quad (8a)$$

$$\times \underbrace{\exp\left(-(\mathbf{x}_A - \hat{\mathbf{x}})\mathbf{S}_A^{-1}(\mathbf{x}_A - \hat{\mathbf{x}})^T\right)}_{\text{Apriori}} \quad (8b)$$

The apriori, Eq. (8b), is necessary as a regularization of this often under-constrained problem and restricts the results using a Gaussian with mean  $\mathbf{x}_A$ , the apriori profile, and the apriori covariance matrix,  $\mathbf{S}_A$ . The noise covariance,  $\mathbf{S}_e$ , describes the Gaussian model of the statistical noise,  $\epsilon$ , on the measurement (with mean  $\bar{\epsilon} = 0$ ).

The noise covariance,  $\mathbf{S}_e$ , is connected to the System-Noise-Temperature, Eq. (2). The apriori profile,  $\mathbf{x}_A$ , is a mean daytime O<sub>3</sub> profile which has been smoothed in order to reflect the low altitude resolution of the data. The apriori covariance matrix ( $\mathbf{S}_A$ -matrix) has been chosen in order to enable the retrieval to reproduce the spectrum to the noise level. In particular, the  $\mathbf{S}_A$ -matrix has only diagonal entries, i.e. inter-layer correlations were not taken into account. The variance is defined to be 20% of the

[Title Page](#)
[Abstract](#)
[Introduction](#)
[Conclusions](#)
[References](#)
[Tables](#)
[Figures](#)
[Back](#)
[Close](#)
[Full Screen / Esc](#)
[Printer-friendly Version](#)
[Interactive Discussion](#)


[Title Page](#)
[Abstract](#)
[Introduction](#)
[Conclusions](#)
[References](#)
[Tables](#)
[Figures](#)
[◀](#)
[▶](#)
[◀](#)
[▶](#)
[Back](#)
[Close](#)
[Full Screen / Esc](#)
[Printer-friendly Version](#)
[Interactive Discussion](#)


O<sub>3</sub> a priori VMR up to an altitude of 40 km and rising from 1.2 ppm at 40 km to 3 ppm at 100 km altitude. The analysis is performed using a pressure grid corresponding to fixed altitude levels from 0.5 km to 100.5 km with a spacing of 1 km. The atmospheric temperature and pressure profile is taken from the ECMWF operational data.

5 Using the Jacobian of the forward model  $F(\mathbf{x}, \mathbf{b})$  with respect to  $\mathbf{x}$ , called the weighting function matrix  $\mathbf{K}$ , the maximum of Eq. (8a) is found by (Rodgers, 2000):

$$\hat{\mathbf{x}} = \mathbf{x}_A + \underbrace{(\mathbf{S}_A^{-1} + \mathbf{K}\mathbf{S}_e\mathbf{K}^T)^{-1}\mathbf{K}^T\mathbf{S}_e}_{\mathbf{D}}(\mathbf{y} - \mathbf{K}\mathbf{x}_A). \quad (9)$$

$\mathbf{D}$  is called the contribution function matrix and can be regarded as the inverse of the weighting function matrix  $\mathbf{K}$ .

10 The setup contains the retrieval of three main parameters:

1. the O<sub>3</sub> atmospheric profile,
2. the continuum absorption of N<sub>2</sub>, O<sub>2</sub> and H<sub>2</sub>O using the model MPM93 (Liebe et al., 1993) and
3. spectral artifacts (e.g. standing waves, offsets due to non-linearities).

#### 15 2.4.2 Performance of the retrieval

The assessment of the retrieval is via the averaging kernel matrix (AVK),  $\mathbf{A}$ , which is defined as:

$$\mathbf{A} = \frac{\partial \hat{\mathbf{x}}}{\partial \mathbf{x}} = \mathbf{D}\mathbf{K} \quad (10)$$

where  $\hat{\mathbf{x}}$  denotes the retrieved quantity and  $\mathbf{x}$  the true quantity of interest. Following Rodgers (2000) the averaging kernel matrix,  $\mathbf{A}$ , can be used to rearrange Eq. (9) to yield an instrument function

$$\hat{\mathbf{x}} = \mathbf{x}_A + \mathbf{A}(\mathbf{x} - \mathbf{x}_A) \quad (11)$$

which describes how the instrument/retrieval “sees” the original quantity of interest.

## 2.5 Error discussion

Following Rodgers (2000) the error in the retrieved profile  $\hat{x}$  can be written as

$$\hat{x} - x = (\mathbf{A} - \mathbf{I})(x - x_A) \quad (12a)$$

$$+ \mathbf{DK}_b(b - \hat{b}) \quad (12b)$$

$$+ \mathbf{D}\Delta F(x, b, \hat{b}) \quad (12c)$$

$$+ \mathbf{D}\epsilon \quad (12d)$$

The vector  $\hat{b}$  holds estimates of the parameters contained in  $b$ .  $\mathbf{K}_b$  denotes the Jacobian of the forward model with respect to the parameters  $b$ .  $\Delta F$  is the difference of the used forward model to the, unknown, true forward model.

### 2.5.1 Smoothing error

The smoothing error, Eq. (12a), is caused by the low altitude resolution of the setup which is equivalent to applying a running weighted average, encoded in the averaging kernels, to the true profile  $x$ . In order to calculate this error, however, knowledge about the statistics of a true ensemble of the  $\text{O}_3$  profile is necessary (Rodgers, 2000, p. 49).

For this data set, it has been decided not to attempt to quantify this error. Instead, the apriori profiles,  $x_A$ , and the averaging kernel matrices,  $\mathbf{A}$ , are explicitly included with the retrieved profiles  $\hat{x}$ , as essential part of the data sets.

### 2.5.2 Forward model parameters

The error caused by uncertainties in the forward model parameters, Eq. (12b), is estimated using the instrument function, Eq. (11). The AVK matrix with respect to the parameters is calculated via:

$$\mathbf{A}_b = \frac{\partial \hat{x}}{\partial b} = \mathbf{DK}_b. \quad (13)$$

Title Page

Abstract

Introduction

Conclusions

References

Tables

Figures

◀

▶

◀

▶

Back

Close

Full Screen / Esc

Printer-friendly Version

Interactive Discussion



Using an estimated covariance matrix for the parameters,  $\mathbf{S}_b$ , the covariance matrix,  $\mathbf{S}_{fp}$ , of the retrieved profile is calculated by

$$\mathbf{S}_{fp} = \mathbf{A}_b^T \mathbf{S}_b \mathbf{A}_b. \quad (14)$$

The standard deviation  $\sigma_{fp}$  of the profile caused by the error in the forward model parameter is

$$\sigma_{fp}^j = \sqrt{\mathbf{S}_{fp}^{jj}} \quad (15)$$

The off-diagonal entries have been neglected.

### 2.5.3 Forward model error

The error caused by a wrong forward model, Eq. (12c), can only be estimated from comparison with independent data. The forward model ARTS which is used here is considered state of the art.

### 2.5.4 Noise error

The noise error is calculated from the measurement noise,  $\mathbf{S}_e$  using Eq. (12d). It is usually the error contribution which is easiest to calculate:

$$\mathbf{S}_\eta = \mathbf{D} \mathbf{S}_e \mathbf{D}^T \quad (16)$$

$$\sigma_\eta^j = \sqrt{\mathbf{S}_\eta^{jj}} \quad (17)$$

### 2.5.5 Summary of error discussion

In Fig. 5 a selection of the errors described above are quantified. This study is restricted to the errors which are caused by wrong spectroscopic parameters. The error due to wrong theoretical assumptions on the spectroscopy itself is difficult to estimate without

Title Page

Abstract

Introduction

Conclusions

References

Tables

Figures

◀

▶

◀

▶

Back

Close

Full Screen / Esc

Printer-friendly Version

Interactive Discussion



---

**OZORAM –  
stratospheric  
O<sub>3</sub> above the Arctic**M. Palm et al.

---

[Title Page](#)[Abstract](#)[Introduction](#)[Conclusions](#)[References](#)[Tables](#)[Figures](#)[⏪](#)[⏩](#)[◀](#)[▶](#)[Back](#)[Close](#)[Full Screen / Esc](#)[Printer-friendly Version](#)[Interactive Discussion](#)

proper spectroscopic measurements. The error figures used for the calculation are summarized in Table 2. The spectroscopic error consists of three parameters, the errors of line intensity,  $I_0$ , pressure broadening parameter,  $\gamma_{\text{AIR}}(T_0)$ , and temperature dependence of the pressure broadening parameter,  $n_{\text{AIR}}$ . The noise error  $\sigma_\eta$  has been calculated for a typical noise value given a measurement time of 1 h. For the total error,  $\sigma_{\text{TOT}}$ , the error contributions have been summed.

From Fig. 5 the following conclusions can be drawn:

1. The error due to a wrong temperature of the cold calibration load,  $\sigma_{T_c}$ , is negligible.
2. The error pattern due to spectral uncertainties,  $\sigma_{f_p}$ , leads to an oscillation in the uncertainty of the retrieved profile (compare discussion in Sect. 5).
3. The spectroscopic error mostly supersedes the error due to measurement noise up to the stratopause. Above the stratopause the measurement error becomes more influential due to the low signal.

## 3 The data set since autumn 2006

### 3.1 Measurement geometry

The direction of the path of view, given by the azimuth angle,  $113^\circ$ , and the polar angle,  $20^\circ$ , has to be taken into account when comparing with models and/or other instruments. See Fig. 6 for a plot of the measurement location and the path of view.

### 3.2 Results

The outstanding features which occur in each of the observed years in the end of winter are filaments of O<sub>3</sub> rich air in the middle stratosphere stretching from the tropics to the poles (comp. Figs. 7 and 8). These events are signs of stratospheric warmings

**OZORAM –  
stratospheric  
O<sub>3</sub> above the Arctic**

M. Palm et al.

at the end of the polar winter, when the polar vortex demises. The down welling of air within the polar vortex (Nash et al., 1996) can be read from the winter 2008/09 data until the mid of January. On the 16 January a major stratospheric warming took place (Labitzke and Kunze, 2009) with a strong enhancement of stratospheric O<sub>3</sub>. After the stratospheric warming the down welling resumes for another month and ceases in a second stratospheric warming in the end of February which marks the end of the vortex.

During the Arctic twilight periods in late autumn and late winter the mesospheric diurnal cycle can clearly be observed (Fig. 9). The O<sub>3</sub> VMR is photochemically controlled at altitudes above 50 km. The O<sub>3</sub> production reaction



is balanced by photolysis



The equilibrium defined by the Reactions (R1) and (R2) depends on the pressure and the illumination of the airmass under consideration. This is reflected by the strong dependency of the O<sub>3</sub> VMR on solar-zenith-angle (SZA) around 60 km altitude. The O<sub>3</sub> VMR is, however, highly variable during the polar night.

### 3.3 A cautionary note

The retrieved profile does not represent reality, especially not at the altitude limits. While the retrieved profile (comp. Fig. 3) shows a deviation from the a priori above 70 km, suggesting such a feature in the real atmosphere state, the AVK (comp. Fig. 4) tell that this is not the case.

This can clearly be seen during the winter 2006/07, where the AVK for retrieval at 70 km altitude is very similar to the AVK kernel for retrieval at 60 km. The retrieval above 60 km altitude is a mixture of profile and columnar information which is defined by the instrument function, Eq. (11).

[Title Page](#)[Abstract](#)[Introduction](#)[Conclusions](#)[References](#)[Tables](#)[Figures](#)[◀](#)[▶](#)[◀](#)[▶](#)[Back](#)[Close](#)[Full Screen / Esc](#)[Printer-friendly Version](#)[Interactive Discussion](#)

The AVK matrix and the apriori are therefore essential parts of the data set. Profiles cannot be interpreted correctly without taking into account the instrument function, Eq. (11).

## 4 Intercomparison of the OZORAM data set

### 4.1 General

The OZORAM profiles are compared to independent data sets. The comparison itself is done via “simulated retrieval” (Rodgers and Connor, 2003). Let  $\hat{\mathbf{x}}_{\text{OR}}$  denote the profiles retrieved from OZORAM measurements and let  $\hat{\mathbf{x}}_{\text{IM}}$  be the profiles from an independent source.

The simulated retrieval,  $\hat{\mathbf{x}}_{\text{SIM}}$ , is the profile the OZORAM would “see” if the independent measurement would represent the true atmosphere (comp. Sect. 4):

$$\hat{\mathbf{x}}_{\text{SIM}} = \mathbf{x}_{\text{OR}}^{\text{A}} + \mathbf{A}_{\text{OR}}(\mathbf{x}_{\text{IM}} - \mathbf{x}_{\text{OR}}^{\text{A}}). \quad (18)$$

The OZORAM retrieval comparing to the simulated retrieval of the independent source yields a set of difference profiles with mean,  $\hat{\boldsymbol{\delta}}_x$ , and covariance  $\mathbf{S}_{\hat{\boldsymbol{\delta}}_x}$ .

$$\hat{\boldsymbol{\delta}}_x = \hat{\mathbf{x}}_{\text{SIM}} - \hat{\mathbf{x}}_{\text{OR}} \quad (19)$$

$$\mathbf{S}_{\hat{\boldsymbol{\delta}}_x} = \mathbf{A}_{\text{OR}}(1 - \mathbf{A}_{\text{IM}})\mathbf{S}_{\text{OR}}\mathbf{A}_{\text{OR}}(1 - \mathbf{A}_{\text{IM}})^T + \mathbf{S}_{\text{OR}} + \mathbf{A}_{\text{OR}}\mathbf{S}_{\text{IM}}\mathbf{A}_{\text{OR}}^T\sigma_x \quad (20)$$

where  $\mathbf{A}_{\text{IM}}$  are the averaging kernels for the independent data sets and the  $\mathbf{S}_{\text{IM}}$  are the error covariance matrices of the independent data.

For the comparison below, the mean difference profile and the standard deviation are normalized to the mean of the retrieved profiles,  $\bar{\mathbf{x}} = 1/N \sum_{i=1}^N \hat{\mathbf{x}}_i$ , in order to yield error in percent:

$$\boldsymbol{\delta} = 2 \frac{\hat{\boldsymbol{\delta}}_x}{(\bar{\mathbf{x}}_{\text{OR}} + \bar{\mathbf{x}}_{\text{IM}})} \times 100\% \quad (21)$$

Title Page

Abstract

Introduction

Conclusions

References

Tables

Figures

◀

▶

◀

▶

Back

Close

Full Screen / Esc

Printer-friendly Version

Interactive Discussion



---

**OZORAM –  
stratomesospheric  
O<sub>3</sub> above the Arctic**M. Palm et al.

---

[Title Page](#)[Abstract](#)[Introduction](#)[Conclusions](#)[References](#)[Tables](#)[Figures](#)[◀](#)[▶](#)[◀](#)[▶](#)[Back](#)[Close](#)[Full Screen / Esc](#)[Printer-friendly Version](#)[Interactive Discussion](#)

Two satellite instruments have been chosen for the comparison, MLS onboard the EOS-AURA satellite and SABER onboard the TIMED satellite. While the first is primarily measuring stratospheric O<sub>3</sub>, the second one is dedicated to mesospheric research. The instruments use different principles to measure O<sub>3</sub>. MLS measures the O<sub>3</sub> emission at 240 GHz. The SABER instrument detects the O<sub>3</sub> emissions in the 9.6 μm band. Both instruments operate in limb geometry.

The OZORAM data have been retrieved using two different spectroscopic data sets, the HITRAN line catalog, version 2004 (Rothman et al., 2005), below called OZORAM-HIT, and the JPL line catalog from 2009 (Pickett et al., 1998), called OZORAM-JPL.

The measurements were compared if the center of ground pixel of the satellite measurement was not further away than 500 km from the point at 60 km altitude measured within 1 h of the OZORAM measurement. A check with a smaller distance between the points of measurement and a shorter coincidence time did not alter the results significantly but reduced the number of matches.

Because of the strong diurnal cycle in the upper stratospheric and mesospheric O<sub>3</sub>, the comparison has been divided into night and day time measurements.

## 4.2 MLS

The OZORAM profiles are compared to the O<sub>3</sub> profiles,  $x_{\text{MLS}}$ , version v2.2, derived from MLS measurements, (Waters et al., 2006).

The independent variable given in the MLS data set is the pressure. Therefore the OZORAM measurements have been interpolated to the pressure grid of the MLS data set. The winter 2008/09 results, mean difference profile  $\delta_x$  and standard deviation  $\sigma_x$  (comp. Eq. 17) are shown in Fig. 10 for OZORAM-HIT (panels a and c), and OZORAM-JPL (panels b and d). The O<sub>3</sub> data derived from the MLS measurements become unreliable above 0.1 hPa (Froidevaux et al., 2008). In comparison to the MLS data, the OZORAM-HIT O<sub>3</sub> profiles show a distinct oscillatory deviation which is a systematic deviation. A similar structure has been reported for ground based microwave data by Boyd et al. (2007) who record the ( $6_{1.5} \rightarrow 6_{0.6}$ ) emission of O<sub>3</sub> at 110.836 GHz and

also compared to MLS data. Boyd et al. (2007) attribute the oscillatory structure to the ground based measurements because the same structure is seen for comparisons with different instruments.

The maxima of the oscillatory structure on the OZORAM measurements are at 1 and 10 hPa and show up in both data sets, OZORAM-HIT and OZORAM-JPL. It can therefore be assumed that the oscillatory structure is inherent to the OZORAM O<sub>3</sub> profiles.

### 4.3 SABER

The independent data comprises O<sub>3</sub> profiles (version 1.07),  $x_{\text{SABER}}$ , derived from the emissions at 9.6  $\mu\text{m}$ . The independent variable for  $x_{\text{SABER}}$  is altitude. Since the SABER altitude grid is finer than the OZORAM one, the data are compared on the altitude grid of the OZORAM.

The SABER profile errors are interpolated from the values given in Table 3. The comparison with SABER profiles,  $x_{\text{SABER}}$ , yields similar results as the comparison to MLS. The general shape of the oscillatory deviation on the retrieved profiles is the same for both instruments, but there is a distinct slope in the difference profiles for the daytime comparison of SABER and OZORAM, Fig. 10g and h. This slope cannot be seen in the other comparisons, especially not in the comparison to the MLS profiles regardless of the spectroscopic data set used.

There is a notable difference between the night time profile comparisons for OZORAM-HIT and OZORAM-JPL, Fig. 10e and f, respectively. The systematic deviation becomes smaller and disappears for altitudes above 60 km for the comparison with OZORAM-JPL.

### 4.4 Intercomparison summary

For the night time measurements, Fig. 10 the comparisons of the satellite are very similar for the OZORAM-JPL data set except for the mesosphere where the performance

## OZORAM – stratospheric O<sub>3</sub> above the Arctic

M. Palm et al.

Title Page

Abstract

Introduction

Conclusions

References

Tables

Figures

◀

▶

◀

▶

Back

Close

Full Screen / Esc

Printer-friendly Version

Interactive Discussion



of the SABER instrument is better the EOS-MLS instrument. This is however to be expected, because of the upper limit if 0.1 hPa for the EOS-MLS measurements.

The similarity in the comparison to the MLS data supports the notion that the reason of the oscillatory deviation should be sought in the OZORAM profiles. Again, the cause of this deviation remains unclear, but the constant deviation above 65 km strongly hint at an error in the forward modeling as is explained further down in Sect. 5.

Based on the comparison described here, the OZORAM retrievals using the JPL spectroscopic data better match the satellite data than OZORAM retrievals using the HITRAN data base in this study.

## 5 On the oscillation in the retrieved profiles

In this section, the oscillatory systematic deviation detected in Sects. 4.2 and 4.3 is investigated.

The regularization by the apriori, which makes similar spectra distinguishable for the retrieval by putting a penalty on unwanted contributions to the retrieved profile, has been checked for effectiveness and compared to systematic spectral errors for the data presented here.

For the check, two typical profiles, a day and a night profile, have been chosen from the SABER data set (Fig. 11, upper row, thin green line). An artificial spectrum has been calculated, using ARTS. These calculations are carried out on a different atmospheric grid than for the retrieval has been used in order to exclude systematic errors due to interpolation. The spectrum has been retrieved 1000 times after degrading it with Gaussian white noise in the range of the measurement noise. The Gaussian noise has been recalculated separately for each retrieval.

The result in Fig. 11, lower row, shows that the regularization works satisfactorily, i.e. no systematic deviation is introduced. The mean difference (black lines) between the artificial profile is Gaussian with zero mean within a 95% confidence interval (the black dashed lines).

Title Page

Abstract

Introduction

Conclusions

References

Tables

Figures

◀

▶

◀

▶

Back

Close

Full Screen / Esc

Printer-friendly Version

Interactive Discussion



---

**OZORAM –  
stratospheric  
O<sub>3</sub> above the Arctic**M. Palm et al.

---

[Title Page](#)[Abstract](#)[Introduction](#)[Conclusions](#)[References](#)[Tables](#)[Figures](#)[⏪](#)[⏩](#)[◀](#)[▶](#)[Back](#)[Close](#)[Full Screen / Esc](#)[Printer-friendly Version](#)[Interactive Discussion](#)

In a second step, three spectral parameters (compare Table 4) have been changed for the calculation of the artificial spectra. The artificial spectra have then been retrieved using the same setup as in the retrievals for the OZORAM-HIT data set.

The systematic deviation introduced by wrong spectral parameters is severe and shows oscillatory patterns. Note in particular the constant deviation in the night time profiles, Fig. 11, lower left plot. The deviation above 65 km that is caused by the change in spectral parameters bears close similarities to the comparison with night time SABER profiles in Fig. 10. The profile information at these altitudes is determined by the Doppler line broadening, which depends on temperature only. The effect is caused by the change of the absorption coefficients in the lower altitudes.

This result calls for a detailed spectroscopic investigation of the 142.176 GHz transition in order to produce high quality spectral data. It has not been attempted to infer the proper line parameters from the satellite measurements because the uncertainties and ad hoc assumptions would make this inferior to laboratory measurements.

## 6 Conclusions

The ground based millimeterwave radiometer OZORAM instrument monitors the O<sub>3</sub> emission line at 142 GHz from the AWIPEV research base on the Spitsbergen archipelago in the high Arctic (79° N) have been described. This work describes the modifications that enable the instrument to measure stratospheric O<sub>3</sub> profiles with a time resolution of about 1 h and a moderate altitude resolution of about 10–20 km (FWHM).

The radiative transfer and the retrieval setup have been summarized and the error budget has been discussed. The error discussion reveals that spectroscopic errors contribute up to 50% to the overall error budget throughout the measurement range.

The data set obtained for Arctic winters 2006/07, 2007/08 and 2008/09 is described and cursorily investigated. This includes a discussion of the measurement geometry, which is important for investigation of processes on short time scales and/or dependent

on solar illumination.

Comparisons with the MLS and the SABER instruments, presented in Sects. 4.2 and 4.3, respectively, show general agreement with at most 20% deviation in the stratosphere and up to 40% deviation in the mesosphere. The comparison yields a distinct systematic oscillatory structure on the OZORAM measurements, which accounts for more than 50% of the discrepancy. This applies for the use of both spectroscopic catalogs, HITRAN and JPL, although the using the JPL catalog produces results closer to satellite measurements in this study. The comparison of OZORAM daytime profiles from with SABER exhibits a distinct mismatch. The SABER instrument detects higher daytime abundance of O<sub>3</sub> than the OZORAM. The difference increases with altitude. Since such a deviation is neither observed in comparison with MLS nor in the night time profile comparison between OZORAM and SABER this may hint at a bias of the daytime profiles derived from SABER. Due to the small number of compared profiles a closer inspection would be desirable.

A further investigation into the oscillatory deviation presents evidence that up to 50% of the deviation between the satellite instruments and OZORAM may be caused by spectroscopic error. The quality of the ground based measurements could thus be considerably improved by finding a better set of spectroscopic parameters, this is, however, out of the scope of this work.

*Acknowledgements.* This study was supported by the DFG priority program CAWSES in the projects SACOSAT I, SACOSAT II and SACOSAT III.

The EOS-MLS data used in this study were acquired as part of the activities of NASA's Science Mission Directorate, and are archived and distributed by the Goddard Earth Sciences (GES) Data and Information Services Center (DISC).

The TIMED-SABER data were retrieved from <ftp://saber.gats-inc.com/>. We thank the science and data processing team of TIMED-SABER.

ECMWF operational data used in this study have been obtained from the ECMWF Data Server. The staff on the AWIPEV research base was very helpful in keeping the instrument running and performing several minor repairs.

## OZORAM – stratomesospheric O<sub>3</sub> above the Arctic

M. Palm et al.

Title Page

Abstract

Introduction

Conclusions

References

Tables

Figures

◀

▶

◀

▶

Back

Close

Full Screen / Esc

Printer-friendly Version

Interactive Discussion



## References

- Benz, A. O., Grigis, P. C., Hungerbühler, V., Meyer, H., Monstein, C., Stuber, B., and Zardet, D.: A broadband FFT spectrometer for radio and millimeter astronomy, *Astron. Astrophys.*, 442, 767–773, doi:10.1051/0004-6361:20053568, 2005. 1937
- 5 Boyd, I. S., Parrish, A. D., Froidevaux, L., von Clarmann, T., Kyrölä, E., III, J. M. R., and Zawodny, J. M.: Ground-based microwave ozone radiometer measurements compared with Aura-MLS v2.2 and other instruments at two Network for Detection of Atmospheric Composition Change sites, *J. Geophys. Res.*, 112, D24S33, doi:10.1029/2007JD008720, 2007. 1948, 1949
- 10 Bühler, S., Eriksson, P., Kuhn, T., von Engel, A., and Verdes, C.: ARTS, the atmospheric radiative transfer simulator, *J. Quant. Spectrosc. Radiat. Transfer*, 91, 65–93, doi:10.1016/j.jqsrt.2004.05.051, 2005. 1938
- Froidevaux, L., Jiang, Y. B., Lambert, A., Livesey, N. J., Read, W. G., Waters, J. W., Browell, E. V., Hair, J. W., Avery, M. A., McGee, T. J., Twigg, L. W., Sumnicht, G. K., Jucks, K. W., 15 Margitan, J. J., Sen, B., Stachnik, R. A., Toon, G. C., Bernath, P. F., Boone, C. D., Walker, K. A., Filipiak, M. J., Harwood, R. S., Fuller, R. A., Manney, G. L., Schwartz, M. J., Daffer, W. H., Drouin, B. J., Cofield, R. E., Cuddy, D. T., Jarnot, R. F., Knosp, B. W., Perun, V. S., Snyder, W. V., Stek, P. C., Thurstans, R. P., and Wagner, P. A.: Validation of Aura Microwave Limb Sounder stratospheric ozone measurements, *J. Geophys. Res.*, 113, D15S20, doi:10. 1029/2007JD008771, 2008. 1948
- 20 Huang, F. T., Mayr III, H. G., J. M. R., Mlynchzak, M. G., and Reber, C. A.: Ozone diurnal variations and mean profiles in the mesosphere, lower thermosphere, and stratosphere, based on measurements from SABER on TIMED, *J. Geophys. Res.*, 113, A04307, doi: 10.1029/2007JA012739, 2008. 1958
- 25 Janssen, M. A. (Ed.): *Atmospheric Remote Sensing by Microwave Radiometry*, John Wiley & Sons, Inc., 1993. 1937, 1938, 1939, 1940, 1941
- Klein, U.: *Aufbau und Betrieb eines breitbandigen, bodengestützten Millimeterwellen-Radiometers zur Messung atmosphärischer Spurenstoffe*, PhD thesis, Universität Bremen, 1993. 1960
- 30 Klein, U., Barry, B., Lindner, K., Wohltmann, I., and Künzi, K. F.: Winter and Spring Observations of Stratospheric Chlorine Monoxide from Ny-Ålesund, Spitsbergen, in 1997/98 and 1998/99, *Geophys. Res. Lett.*, 27, 4093–4097, 2000. 1956

AMTD

3, 1933–1970, 2010

---

### OZORAM – stratospheric O<sub>3</sub> above the Arctic

M. Palm et al.

---

Title Page

Abstract

Introduction

Conclusions

References

Tables

Figures

◀

▶

◀

▶

Back

Close

Full Screen / Esc

Printer-friendly Version

Interactive Discussion



- Klein, U., Wohltmann, I., Lindner, K., and Künzi, K. F.: Ozone depletion and chlorine activation in the Arctic winter 1999/2000 observed in Ny-Ålesund, *J. Geophys. Res.*, 107, 8288, doi:10.1029/2001JD000543, 2002. 1956
- Labitzke, K. and Kunze, M.: On the remarkable Arctic winter in 2008/2009, *J. Geophys. Res.*, 114, D00I02, doi:10.1029/2009JD012273, 2009. 1946
- Lary, D. J.: Catalytic destruction of stratospheric ozone, *J. Geophys. Res.*, 102, 21515–21526, 1997. 1935
- Liebe, H. J., Hufford, G. A., and Cotton, M. G.: Propagation modeling of moist air and suspended water/ice particles at frequencies below 1000 GHz, in: Proc. AGARD 52nd Spec. Meeting EM Wave Propag. Panel, pp. 3.1–3.10., Palma De Maiorca, Spain, 1993. 1942
- Nash, E. R., Newman, P., Rosenfeld, J. E., and Schoeberl, M. R.: An objective determination of the polar vortex using Ertel's potential vorticity, *J. Geophys. Res.*, 101, 9471–9478, 1996. 1946
- Pickett, H. M., Poynter, R. L., Cohen, E. A., Delitsky, M. L., Pearson, J. C., and Muller, H. S. P.: Submillimeter, Millimeter, and Microwave Spectral Line Catalog, *J. Quant. Spectrosc. Rad. Transfer*, 60, 883–890, 1998. 1939, 1948
- Randall, C. E., Harvey, V. L., Manney, G. L., Orsolini, Y., Codrescu, M., Sioris, C., Brohede, S., Haley, C. S., Gordley, L. L., Zawodny, J. M., and III, J. M. R.: Stratospheric effects of energetic particle precipitation in 2003–2004, *Geophys. Res. Lett.*, 32, L05802, doi:10.1029/2004GL022003, 2005. 1935
- Rodgers, C. D.: *Inverse Methods for Atmospheric Sounding*, World Scientific Publishing Co. Pte. Ltd., 2000. 1941, 1942, 1943
- Rodgers, C. D. and Connor, B. J.: Intercomparison of remote sounding instruments, *J. Geophys. Res.*, 108, 4116, doi:10.1029/2002JD002299, 2003. 1947
- Rothman, L. S., Jacquemart, D., Barbe, A., Benner, D. C., Birk, M., Brown, L. R., Carleer, M. R., Chackerian, C., Chance, K., Coudert, L. H., Dana, V., Devi, V. M., Flaud, J. M., Gamache, R. R., Goldman, A., Hartmann, J. M., Jucks, K. W., Maki, A. G., Mandin, J. Y., Massie, S. T., Orphal, J., Perrin, A., Rinsland, C. P., Smith, M. A. H., Tennyson, J., Tolchenov, R. N., Toth, R. A., Vander Auwera, J., Varanasi, P., and Wagner, G.: The HITRAN 2004 molecular spectroscopic database, *J. Quant. Spectr. Radiat. Trans.*, 96, 139–204, 2005. 1939, 1948
- Russel, J., Mlynczak, M., and Gordley, L.: An Overview of the SABER Experiment for the TIMED Mission, in: *Optical Spectroscopic Techniques and Instrumentation for Atmospheric and Space Research*, edited by: Wang, J. and Hays, P. B., vol. 2266 of *Proceedings of the*

---

**OZORAM –  
stratospheric  
O<sub>3</sub> above the Arctic**M. Palm et al.

---

[Title Page](#)[Abstract](#)[Introduction](#)[Conclusions](#)[References](#)[Tables](#)[Figures](#)[◀](#)[▶](#)[◀](#)[▶](#)[Back](#)[Close](#)[Full Screen / Esc](#)[Printer-friendly Version](#)[Interactive Discussion](#)

*Society of Photo-Optical Instrumentation Engineers (SPIE)*, pp. 406–415, SOC Photo Opt Instrumentation Engineers, SPIE – Int. Soc. Optical Engineering, P.O. Box 10, Bellingham, WA 98227-0010, Optical Spectroscopic Techniques and Instrumentation for Atmospheric and Space Research Conference, San Diego, CA, 25–27 July 1994. 1936

- 5 Schieder, R. and Kramer, C.: Optimization of heterodyne observations using Allan variance measurements, *Astron. Astrophys.*, 373, 746–756, 2001.
- Schoeberl, M. R., Douglass, A. R., Hilsenrath, E., Bhartia, P. K., Beer, R., Waters, J. W., Gunson, M. R., Froidevaux, L., Gille, J. C., Barnett, J. J., Levelt, P. E., and DeCola, P.: Overview of the EOS Aura Mission, *IEEE Trans. Geosci. Rem. Sens.*, 44, 1066–1074, doi: 10.1109/TGRS.2005.861950, 2006. 1936
- 10 Sinnhuber, B.-M., Langer, J., Klein, U., Raffalski, U., Künzi, K., and Schrems, O.: Ground based millimeter-wave observations of Arctic ozone depletion during winter and spring of 1996/97, *Geophys. Res. Lett.*, 25, 3227–3330, doi:10.1029/98GL52488, 1998. 1936, 1956
- 15 Waters, J., Froidevaux, L., Harwood, R., Jarnot, R., Pickett, H., Read, W., Siegel, P., Cofield, R., Filipiak, M., Flower, D., Holden, J., Lau, G., Livesey, N., Manney, G., Pumphrey, H., Santee, M., Wu, D., Cuddy, D., Lay, R., Loo, M., Perun, V., Schwartz, M., Stek, P., Thurstans, R., Boyles, M., Chandra, K., Chavez, M., Chen, G., Chudasama, B., Dodge, R., Fuller, R., Girard, M., Jiang, J., Jiang, Y., Knosp, B., LaBelle, R., Lam, J., Lee, K., Miller, D., Oswald, J., Patel, N., Pukala, D., Quintero, O., Scaff, D., Van Snyder, W., Tope, M., Wagner, P., and Walch, M.: The Earth Observing System Microwave Limb Sounder (EOS MLS) on the Aura satellite, *IEEE T. Geosci. Remote.*, 44, 1075–1092, doi:10.1109/TGRS.2006.873771, 2006. 1948
- 20

AMTD

3, 1933–1970, 2010

---

**OZORAM –  
stratospheric  
O<sub>3</sub> above the Arctic**

M. Palm et al.

---

Title Page

Abstract

Introduction

Conclusions

References

Tables

Figures

◀

▶

◀

▶

Back

Close

Full Screen / Esc

Printer-friendly Version

Interactive Discussion



## OZORAM – stratospheric O<sub>3</sub> above the Arctic

M. Palm et al.

**Table 1.** Summary of the characteristics of the OZORAM. The altitude range and the altitude resolution depend on integration time. The numbers given correspond to an measurement interval of 1 h. For the difference in altitude range refer to Sect. 2.2. The data recorded until 2004 have been used in past publications (Sinnhuber et al., 1998; Klein et al., 2000, 2002) and are listed here for completeness.

	pre 2004	2006–2007	2007–2008	from 2008
Backend	AOS	AOS + CTS	FFTS	FFTS
Sys. NT	3500 K	1100 K	1100 K	1100 K
Band width	1.5 GHz	1 GHz	0.5 GHz	0.8 GHz
Resolution	1.5 MHz	1.5 MHz + 10 kHz	60 kHz	60 kHz
Alt. range	15–40 km	15–60 km	30–60 km	25–70 km

Title Page

Abstract

Introduction

Conclusions

References

Tables

Figures

◀

▶

◀

▶

Back

Close

Full Screen / Esc

Printer-friendly Version

Interactive Discussion



## OZORAM – stratospheric O<sub>3</sub> above the Arctic

M. Palm et al.

**Table 2.** Input for error calculation plotted in Fig. 5 for the O<sub>3</sub> line at 142.176 GHz line.

Quantity	Symbol used	Error reported in reference	Reference	Error assumed in this work
Line intensity	$I_0$	unavailable	HITRAN	5%
Pressure broadening	$\gamma_{\text{AIR}}(T_0)$	$5\% \leq \sigma_{\gamma_{\text{AIR}}(T_0)} < 10\%$	HITRAN	5%
Temperature dependency of $\gamma_{\text{AIR}}(T_0)$	$n_{\text{AIR}}$	$10\% \leq \sigma_{n_{\text{AIR}}} < 20\%$	HITRAN	10%
Temperature profile	$T$	none	none	5 %
Temperature of cold calibration load	$T_c$	1%	Manual of sensor	1%

Title Page

Abstract

Introduction

Conclusions

References

Tables

Figures

◀

▶

◀

▶

Back

Close

Full Screen / Esc

Printer-friendly Version

Interactive Discussion



**OZORAM –  
stratomesospheric  
O<sub>3</sub> above the Arctic**

M. Palm et al.

[Title Page](#)[Abstract](#)[Introduction](#)[Conclusions](#)[References](#)[Tables](#)[Figures](#)[Back](#)[Close](#)[Full Screen / Esc](#)[Printer-friendly Version](#)[Interactive Discussion](#)**Table 3.** Errors defined for the SABER data set. The error figures follow Huang et al. (2008).

Altitude [km]	10	50	60	100
Error [%]	10	10	20	40

**OZORAM –  
stratospheric  
O<sub>3</sub> above the Arctic**

M. Palm et al.

**Table 4.** Change of spectral parameter in study of the oscillatory error pattern in Sect. 5. The range of the disturbances is in the mid of the error ranges given in the HITRAN database (compare Table 2). The line intensity is assumed to be known to a high precision (M. Birk, oral communication).

Quantity	Change by [%]
Pressure broadening	+7.5
Temperature dependency of pressure broadening	–15
Line intensity	+1

[Title Page](#)[Abstract](#)[Introduction](#)[Conclusions](#)[References](#)[Tables](#)[Figures](#)[◀](#)[▶](#)[◀](#)[▶](#)[Back](#)[Close](#)[Full Screen / Esc](#)[Printer-friendly Version](#)[Interactive Discussion](#)

**OZORAM –  
stratospheric  
O<sub>3</sub> above the Arctic**

M. Palm et al.

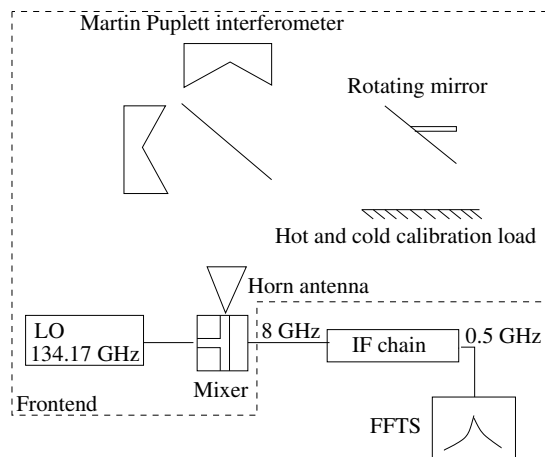


**Fig. 1.** Overview sketch of the OZORAM. Technical details are described in Klein (1993) and have been omitted for clarity. The dashed line encloses the frontend with the quasi optical system and the first mixing stage.

[Title Page](#)[Abstract](#)[Introduction](#)[Conclusions](#)[References](#)[Tables](#)[Figures](#)[◀](#)[▶](#)[◀](#)[▶](#)[Back](#)[Close](#)[Full Screen / Esc](#)[Printer-friendly Version](#)[Interactive Discussion](#)

**OZORAM –  
stratospheric  
O<sub>3</sub> above the Arctic**

M. Palm et al.

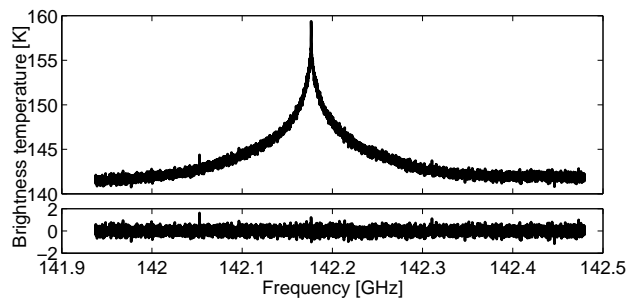


**Fig. 2.** A spectrum measured on the 14 December 2008, 08:30 a.m.–09:30 a.m. The lower figure shows the residuum after profile retrieval (comp. Fig. 3).

[Title Page](#)[Abstract](#)[Introduction](#)[Conclusions](#)[References](#)[Tables](#)[Figures](#)[◀](#)[▶](#)[◀](#)[▶](#)[Back](#)[Close](#)[Full Screen / Esc](#)[Printer-friendly Version](#)[Interactive Discussion](#)

**OZORAM –  
stratospheric  
O<sub>3</sub> above the Arctic**

M. Palm et al.

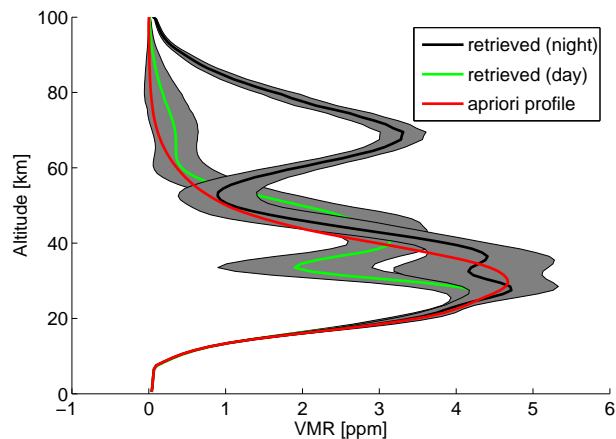


**Fig. 3.** O<sub>3</sub> profiles retrieved during night (black) and day (green). The spectrum shown in Fig. 2 corresponds to the night time spectrum. The grey shaded region is the uncertainty caused by the total error as derived in Sect. 2.5.

[Title Page](#)[Abstract](#)[Introduction](#)[Conclusions](#)[References](#)[Tables](#)[Figures](#)[◀](#)[▶](#)[◀](#)[▶](#)[Back](#)[Close](#)[Full Screen / Esc](#)[Printer-friendly Version](#)[Interactive Discussion](#)

OZORAM –  
stratospheric  
O<sub>3</sub> above the Arctic

M. Palm et al.

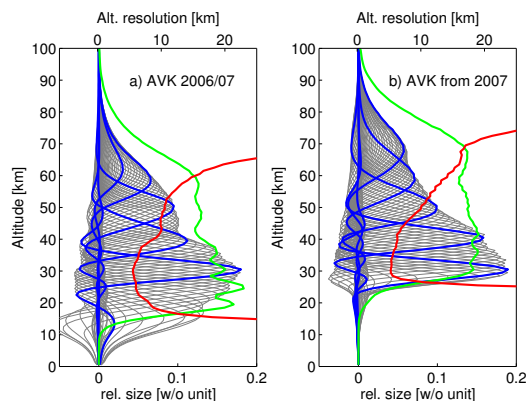


**Fig. 4.** Averaging kernels for the periods 2006/07 **(a)** and 2008 **(b)** onwards. The thick blue lines are the averaging kernels for the values at 30, 40, 50, 60, 70 km altitude. The solid green line is the sum of the AVK, divided by 10 for visualization. The solid red line is the altitude resolution (FWHM of the Gaussian approximation to the AVK) for the corresponding altitude with the axis at the top of the figures. The differences in the AVKs reflect the hardware changes as described in Sect. 2.2.

[Title Page](#)[Abstract](#)[Introduction](#)[Conclusions](#)[References](#)[Tables](#)[Figures](#)[◀](#)[▶](#)[◀](#)[▶](#)[Back](#)[Close](#)[Full Screen / Esc](#)[Printer-friendly Version](#)[Interactive Discussion](#)

## OZORAM – stratospheric O<sub>3</sub> above the Arctic

M. Palm et al.

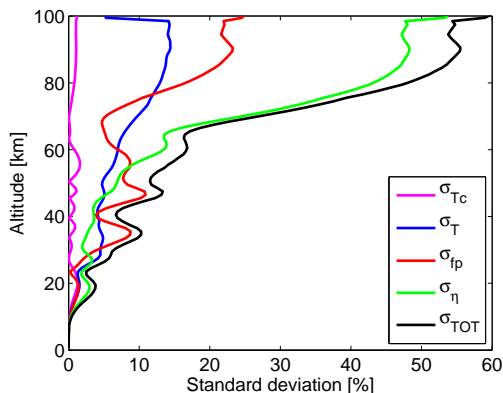


**Fig. 5.** Uncertainty in the profile due to errors in the instrumental parameters and spectroscopy. The plot covers random error due to noise on the spectra,  $\sigma_{\eta}$ , and systematic error due to deviations in the temperature of the cold calibration load,  $\sigma_{TC}$ , in the atmospheric temperature profile,  $\sigma_T$ , the pressure broadening, its temperature coefficient, and the line intensity,  $\sigma_{fp}$ . The sum of those errors is  $\sigma_{TOT} = \sqrt{\sigma_{TC}^2 + \sigma_T^2 + \sigma_{fp}^2 + \sigma_{\eta}^2}$ .

Title Page

Abstract

Introduction

Conclusions

References

Tables

Figures

◀

▶

◀

▶

Back

Close

Full Screen / Esc

Printer-friendly Version

Interactive Discussion



**OZORAM –  
stratospheric  
O<sub>3</sub> above the Arctic**

M. Palm et al.

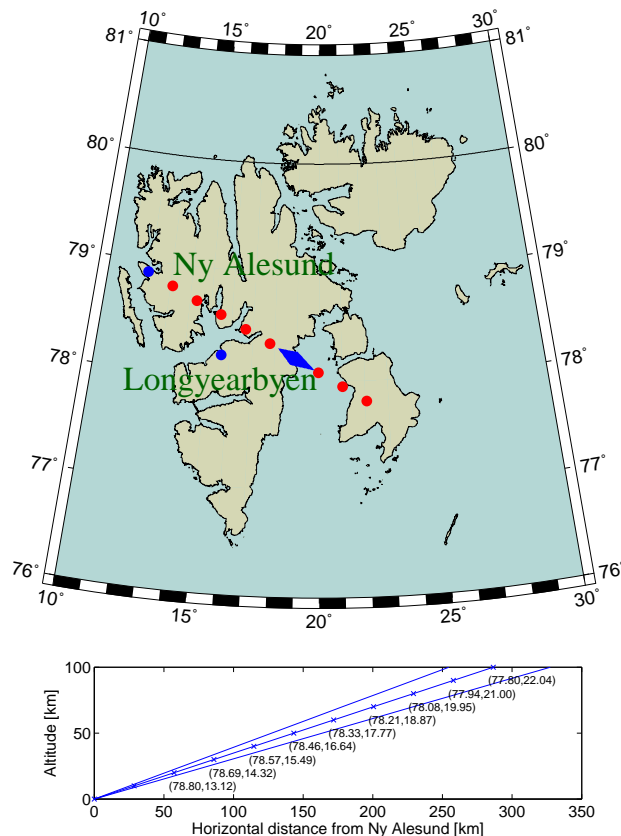


**Fig. 6.** OZORAM measurement geometry. The upper panel shows the ground track of the path of view. The dots denote the path of view in 10 km steps. The lower panel denotes the path of view in the plane given by azimuth and zenith directions.

[Title Page](#)[Abstract](#)[Introduction](#)[Conclusions](#)[References](#)[Tables](#)[Figures](#)[◀](#)[▶](#)[◀](#)[▶](#)[Back](#)[Close](#)[Full Screen / Esc](#)[Printer-friendly Version](#)[Interactive Discussion](#)

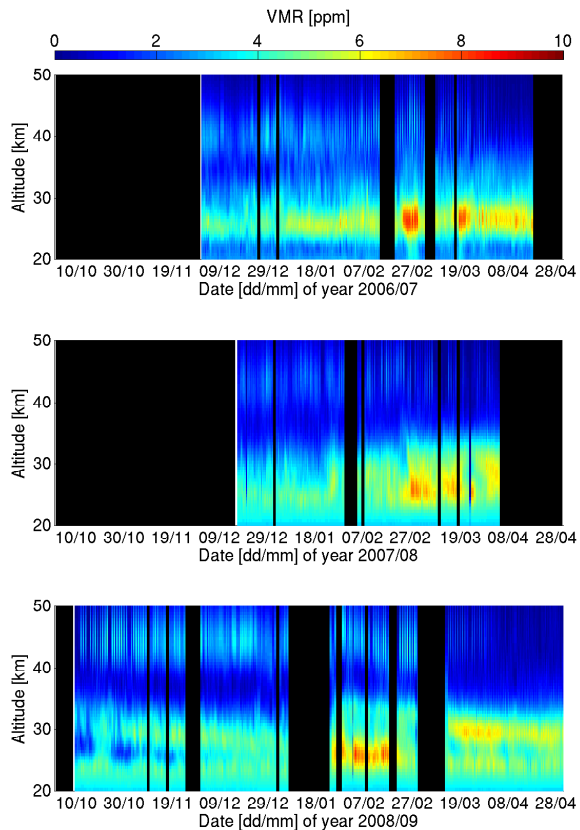


**Fig. 7.** Measurements of three winters, 2006/07 2007/08 and 2008/09. The dates are centered solstice each winter in order to make features comparable. Data gaps of more than one day have been blackened. For the actual altitude range and the altitude resolution refer to text Sect. 3.

**OZORAM –  
stratospheric  
O<sub>3</sub> above the Arctic**

M. Palm et al.

Title Page

Abstract

Introduction

Conclusions

References

Tables

Figures

⏪

⏩

◀

▶

Back

Close

Full Screen / Esc

Printer-friendly Version

Interactive Discussion



**OZORAM –  
stratospheric  
O<sub>3</sub> above the Arctic**

M. Palm et al.

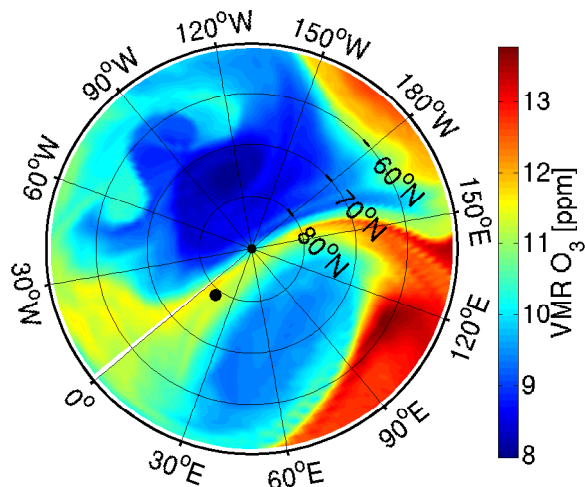


**Fig. 8.** The O<sub>3</sub> field at about 30 km from ECMWF operational analysis on the 1 March 2008, 00:00:00 UTC. It can clearly be seen that a filament of O<sub>3</sub> rich air stretches from the tropics over the pole. The position of Ny-Ålesund is marked with a black disk. The filament can also be seen in the OZORAM measurements (compare Fig. 7).

[Title Page](#)[Abstract](#)[Introduction](#)[Conclusions](#)[References](#)[Tables](#)[Figures](#)[◀](#)[▶](#)[◀](#)[▶](#)[Back](#)[Close](#)[Full Screen / Esc](#)[Printer-friendly Version](#)[Interactive Discussion](#)

**OZORAM –  
stratomesospheric  
O<sub>3</sub> above the Arctic**

M. Palm et al.

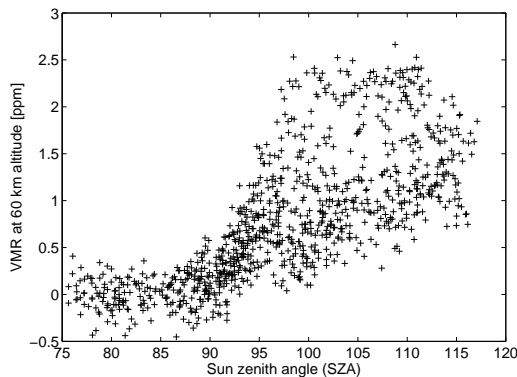


**Fig. 9.** The dependency on solar zenith angle (SZA) of mesospheric O<sub>3</sub> at 60 km altitude above Spitsbergen. For 90° SZA the sun is leveled with the horizon, 0° is equivalent with the sun directly above the observer. Compare text for a more detailed discussion. The negative values for SZA < 95° are caused by the uncertainty in the retrieval (values below zero are not suppressed).

[Title Page](#)[Abstract](#)[Introduction](#)[Conclusions](#)[References](#)[Tables](#)[Figures](#)[⏪](#)[⏩](#)[◀](#)[▶](#)[Back](#)[Close](#)[Full Screen / Esc](#)[Printer-friendly Version](#)[Interactive Discussion](#)

## OZORAM – stratospheric O<sub>3</sub> above the Arctic

M. Palm et al.

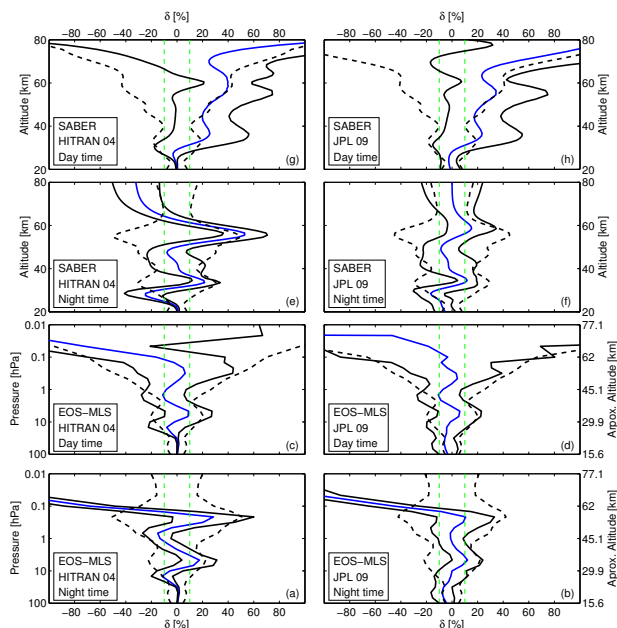


**Fig. 10.** Intercomparison of the OZORAM data set, using HITRAN 2004 (left column) or JPL 2009 spectroscopy (right column), respectively, to the measurements of EOS-MLS (IM = MLS; lower two rows) and SABER (IM = SABER; upper two rows). The plots show the mean difference  $\delta = 200 \cdot (\hat{x}_{IM} - \hat{x}_{OR}) / (\hat{x}_{IM} + \hat{x}_{OR})$  (solid blue; comp. Sect. 4.1). The standard deviation of the difference of the measurements is denoted by the solid black lines, the dashed black lines denote the theoretical error of the difference. This error is caused by the standard deviation of the measurements themselves, Eq. (20). The dashed green lines mark the 10% range.

Title Page

Abstract

Introduction

Conclusions

References

Tables

Figures

◀

▶

◀

▶

Back

Close

Full Screen / Esc

Printer-friendly Version

Interactive Discussion



## OZORAM – stratospheric O<sub>3</sub> above the Arctic

M. Palm et al.

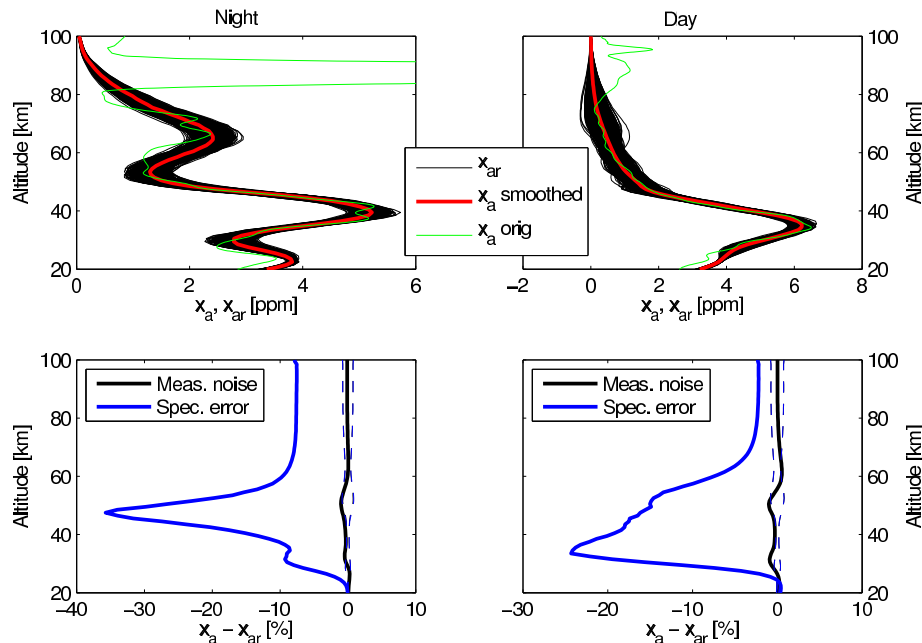


**Fig. 11.** Influence of systematic errors on the profile using selected spectral data. The figures in the upper row show the profiles taken as typical profiles (solid green) for night (right side) and day (left side). Solid red lines denote the same profiles after convolving with OZORAM averaging kernels. The thin black lines represent retrieved profiles with unchanged spectroscopy. These vary due to statistical noise used to degrade the artificial spectrum. The figures in the lower row show statistical properties of the retrievals. The solid lines denote the mean of the difference artificial profile,  $x_a$ , minus retrieved artificial profile,  $x_{ar}$ . The dashed lines denote the confidence interval of the zero difference (95%). The deviation caused by wrong spectral parameters is plotted in blue lines.

[Title Page](#)
[Abstract](#)
[Introduction](#)
[Conclusions](#)
[References](#)
[Tables](#)
[Figures](#)
[⏪](#)
[⏩](#)
[◀](#)
[▶](#)
[Back](#)
[Close](#)
[Full Screen / Esc](#)
[Printer-friendly Version](#)
[Interactive Discussion](#)
